This is an open access article published under a Creative Commons Non-Commercial No Derivative Works (CC-BY-NC-ND) Attribution License, which permits copying and redistribution of the article, and creation of adaptations, all for non-commercial purposes.

Biochemistry

Article

Cite This: Biochemistry 2017, 56, 5991-6005

pubs.acs.org/biochemistry

Metal Dependence of the Xylose Isomerase from *Piromyces* sp. E2 Explored by Activity Profiling and Protein Crystallography

Misun Lee,[†] Henriëtte J. Rozeboom,[†] Paul P. de Waal,[‡] Rene M. de Jong,[‡] Hanna M. Dudek,[†,§] and Dick B. Janssen*[,†]

[†]Biochemical Laboratory, Groningen Biomolecular Sciences and Biotechnology Institute, University of Groningen, Nijenborgh 4, 9747 AG Groningen, The Netherlands

[‡]DSM Biotechnology Center, Alexander Fleminglaan 1, 2613 AX Delft, The Netherlands

Supporting Information

ABSTRACT: Xylose isomerase from *Piromyces* sp. E2 (PirXI) can be used to equip *Saccharomyces cerevisiae* with the capacity to ferment xylose to ethanol. The biochemical properties and structure of the enzyme have not been described even though its metal content, catalytic parameters, and expression level are critical for rapid xylose utilization. We have isolated the enzyme after high-level expression in *Escherichia coli*, analyzed the metal dependence of its catalytic properties, and determined 12 crystal structures in the presence of different metals, substrates, and substrate analogues. The activity assays revealed that various bivalent metals can activate PirXI for xylose isomerization. Among these metals, Mn^{2+} is the most favorable for catalytic activity. Furthermore, the enzyme shows the highest affinity for Mn^{2+}, which was established by measuring the activation constants (K_{act}) for different metals. Metal analysis of the purified enzyme showed that *in vivo* the enzyme binds a mixture of metals that is determined by metal availability as well as affinity, indicating that the native metal composition can influence activity. The crystal structures show the presence of an active site similar to that of other xylose isomerases, with a D-xylose binding site containing two tryptophans and a catalytic histidine, as well as two metal binding sites that are formed by carboxylate groups of conserved aspartates and glutamates. The binding positions and conformations of the metal-coordinating residues varied slightly for different metals, which is hypothesized to contribute to the observed metal dependence of the isomerase activity.

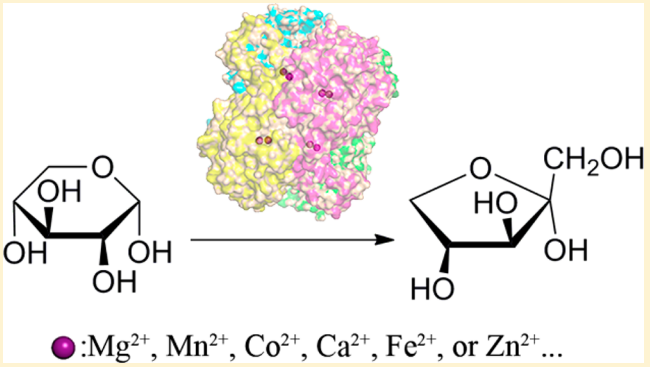

Cost-effective production of second-generation bioethanol requires maximal utilization of sugars present in cellulosic biomass, because raw materials account for approximately one-third of the overall production cost.[1] Besides D-glucose, the most abundant monosaccharide in lignocellulose and hemicellulose is D-xylose, and fermentation of xylose along with glucose would significantly increase the total ethanol yield.[2] For such simultaneous fermentation of glucose and xylose, *Saccharomyces cerevisiae* would be a particularly attractive organism as it is an established ethanol producer that is not very vulnerable to inhibitors present in cellulose hydrolysates and shows a relatively high tolerance to extracellular ethanol.[1] However, natural strains of *S. cerevisiae* do not metabolize xylose, because of its inability to convert D-xylose to D-xylulose, an aldose to ketose isomerization reaction. Because D-xylulose can be metabolized, research has been devoted to engineer yeast variants that express a heterologous xylose isomerase for catalyzing this reaction.[3−6] Alternatively, xylose isomerization can be achieved by incorporating both a xylose reductase and a xylitol dehydrogenase,[7] although this is not preferred because it could cause a cellular cofactor imbalance.[8,9] Because xylose isomerase requires only metal cofactors, it offers the most attractive solution. Furthermore, the use of an isomerase rather than dehydrogenases prevents the formation of xylitol, which may emerge as an unwanted side product.[10]

Xylose isomerases and related glucose isomerases have been studied for decades because of their application as glucose isomerases in the production of high-fructose corn syrups from starch hydrolysates.[11] The use of the enzymes in ethanol-producing yeasts has been more recent. Isomerases from different bacterial sources, including *Escherichia coli*, *Actinoplanes missouriensis*, *Streptomyces rubiginosus*, *Bacillus subtilis*, and *Clostridium thermosulfurogenes*, have been tested, but functional expression in *S. cerevisiae* appeared to be problematic.[12−15] Xylose isomerase from *Thermus thermophilus* was functionally expressed in *S. cerevisiae*, but the enzyme from this thermophilic organism showed very low activity at 30 °C.[16]

The first eukaryotic XI gene that could be expressed well in its active form in *S. cerevisiae* was obtained from the anaerobic fungus *Piromyces* sp. E2 (PirXI), and its expression in an *S.*

Received: August 13, 2017
Revised: October 13, 2017
Published: October 18, 2017

© 2017 American Chemical Society

DOI: 10.1021/acs.biochem.7b00777
Biochemistry 2017, 56, 5991−6005

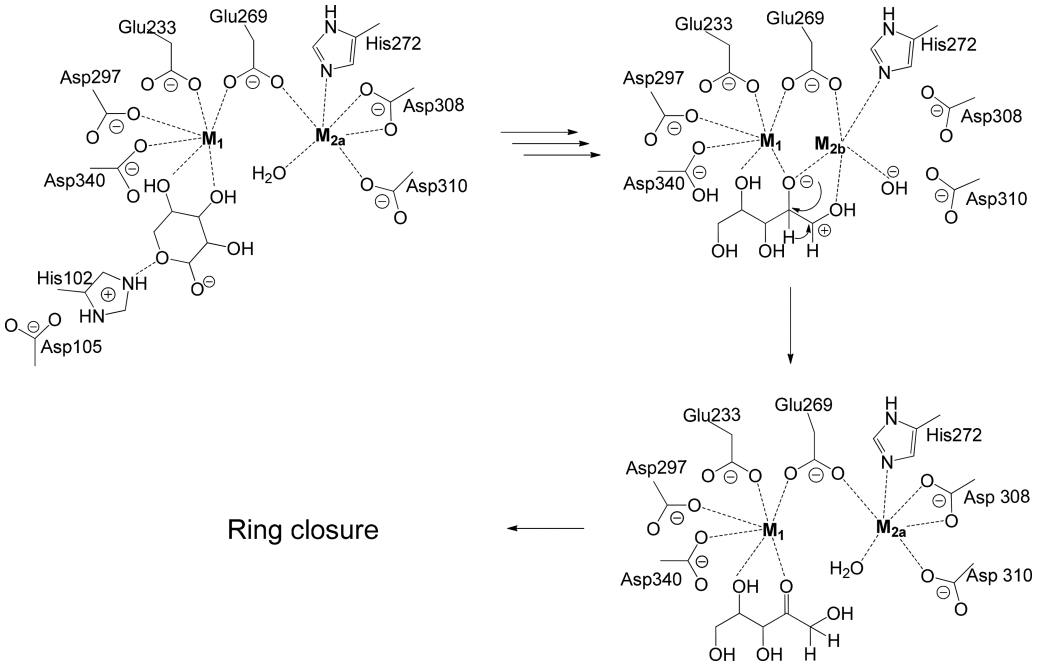

Figure 1. Mechanism of conversion D-xylose to D-xylulose.[25,26] Linearization of D-xylose catalyzed by His102/Asp105 is followed by movement of the catalytic metal from position M2a to position M2b, where it coordinates with O1 and O2 of the sugar. A proton is transferred from O2 to O1, and a hydride shifts from C2 to C1. D-Xylulose is formed by ring closure.

cerevisiae enabled the fermentation of xylose to ethanol.[5,17,18] Although later a few xylose isomerases from other sources were also expressed in *S. cerevisiae*,[3,4,6,19,20] xylose-based growth rates and ethanol production levels do not exceed those found for the *S. cerevisiae* expressing XI from *Piromyces* sp. E2.[18] A further improved *S. cerevisiae* strain equipped with PirXI indeed showed high ethanol production yields, reaching almost the theoretical level, and the use of xylose isomerase appears to be preferable over the combination of a xylose reductase and a xylitol dehydrogenase allowing isomerization via xylitol.[10,20]

In spite of these promising achievements, there is significant room to improve the anaerobic metabolism of xylose. Engineering of the strain by overexpressing the non-oxidative pentose phosphate pathway enzymes may enhance the growth rate.[20,21] Evolutionary optimization can also improve the rate of xylose consumption.[22,23] In such improved *S. cerevisiae* strains, a very high expression level of PirXI is still required for growth on xylose, especially for anaerobic metabolism, and in such evolved strains, PirXI may be the major intracellular protein (unpublished data). This must be an energetic burden to the cells and also indicates that xylose isomerization still is the rate-limiting step in engineered strains that have lower expression levels of xylose isomerase. No detectable accumulation of the product xylulose in an anaerobic culture of an engineered and PirXI-expressing strain growing on xylose was found, further suggesting that PirXI activity is limiting xylose metabolism.[21] Therefore, engineering of PirXI to enhance its activity will further improve xylose utilization. A directed evolution study using error-prone polymerase chain reaction showed that a more active xylose isomerase could enhance the growth of *S. cerevisiae* on xylose.[24] Further progress and more focused engineering of the enzyme are hampered by the lack of a description of the biochemical properties of PirXI and the absence of structural information.

Xylose isomerases are tetrameric enzymes that require two bivalent metals to catalyze the isomerization of the aldose D-xylose to the ketose D-xylulose (Figure 1). One of them is often described as the structural metal as it is involved in the proper binding of the substrate and the other as the catalytic metal as it is critical for the isomerization reaction.[27] The activity of xylose isomerase is reported to be influenced by the type of metal that is bound. For example, Mg^{2+}, Co^{2+}, and Mn^{2+} are known to be activators, and Ni^{2+}, Cu^{2+}, Zn^{2+}, Ca^{2+}, and Fe^{2+} mostly act as inhibitors.[26,28−30] Although the active sites of xylose isomerases are highly conserved, the metal preferences of the enzymes vary. Some XIs seems to be most active with Mg^{2+}, while others show the highest activity with Mn^{2+}.[28,31,32] The importance of the metal dependence for *in vivo* conversion of D-xylose was recently discovered in a study showing that mutations influencing metal homeostasis through inactivation of the PMR1 gene increase the relative Mn^{2+} content of *S. cerevisiae* cells and of the expressed PirXI.[33]

XIs can be divided into two structural types, i.e., class I and class II enzymes. The major difference between the two classes is an N-terminal extension in class II xylose isomerases. From sequence analysis, the PirXI enzyme explored here appears to be a class II xylose isomerase. Currently, only a few class II XI structures are available,[34] and these have no bound substrates, unlike structures for class I XIs that have been obtained with different ligands.

In this study, we describe the catalytic properties of PirXI expressed in *E. coli*. We also examined the metal specificity of the enzyme by measuring catalytic activities and affinities with a range of different metals that might be present in the cytosol of *S. cerevisiae* during the fermentation process. Furthermore, we report several structures of the class II XI from *Piromyces*, determined by X-ray crystallography, with various combinations of metals (Mg^{2+}, Mn^{2+}, Co^{2+}, Fe^{2+}, Ca^{2+}, Ni^{2+}, and Cd^{2+}) and substrate (xylose), product (xylulose), or inhibitor (xylitol or sorbitol). The results indicate that small differences in metal−protein interactions influence the position and reactivity of bound metals.

DOI: 10.1021/acs.biochem.7b00777
Biochemistry 2017, 56, 5991−6005

MATERIALS AND METHODS

Expression of PirXI in *E. coli*. A synthetic *xylA* gene encoding XI from *Piromyces* sp. E2 (GenBank accession number AJ249909) was obtained from GenScript USA Inc. (Piscataway, NJ). The sequence was codon-optimized for expression in *E. coli*. The *xylA* gene was cloned into a pBAD/myc-His-derived plasmid (Invitrogen). In this plasmid, the original NdeI sites were removed and the NcoI site was replaced with an NdeI site. The *xylA* gene was cloned using NdeI and HindIII sites with insertion of a stop codon at the end of the *xylA* coding sequence. The obtained pBAD-PirXI plasmid was transformed into *E. coli* Top10 (Invitrogen) or NEB 10-β (New England Biolabs). The sequence of the plasmid was verified by sequencing.

For expression of XI, *E. coli* Top10 cells or NEB 10-β cells harboring the pBAD-PirXI plasmid were cultivated in TB medium (12 g/L tryptone, 24 g/L yeast extract, 5 mL/L glycerol, 2.31 g/L KH_2PO_4, and 16.43 g/L $K_2HPO_4{\cdot}3H_2O$) supplemented with 50 μg mL^{-1} ampicillin and 0.2% (w/v) L-arabinose for 16 h at 37 °C. The cells were harvested by centrifugation, washed with 20 mM Tris-HCl (pH 8.5), and directly used for enzyme purification or stored at −20 °C until further use.

Purification of XI Overexpressed in *E. coli*. The cells were disrupted by sonication, and cell debris was removed by centrifugation for 45 min at 31000*g* and 4 °C. The supernatant was applied to a Q-sepharose Fast Flow resin (GE Healthcare) equilibrated with 20 mM Tris-HCl (pH 8.5) in a gravity flow column and incubated for 30 min at 4 °C in a rotating format. The column was washed with 15 column volumes of 20 mM Tris-HCl (pH 8.5). Then xylose isomerase was eluted from the column using 20 mM Tris-HCl (pH 8.5) containing 100 mM KCl. Fractions containing protein were pooled and desalted using an EconoPac 10-DG desalting column (Bio-Rad) pre-equilibrated with 10 mM MOPS (pH 7.0). Protein concentrations were determined using the theoretical extinction coefficient at 280 nm ($\varepsilon_{280,XI}$ = 73800 M^{-1} cm^{-1}) calculated by the ProtParam tool (http://web.expasy.org/protparam/). The protein was stable when it was stored at 4 °C for several weeks. For long-term storage, the protein was frozen in liquid nitrogen and stored at −80 °C.

Activity Assays. Most assays were performed using the enzyme with a controlled metal composition. For this, we first prepared the apoenzyme by buffer exchange with 10 mM EDTA in 10 mM Tris-HCl (pH 8.0) using either dialysis or EconoPac 10-DG desalting columns (Bio-Rad). The samples were incubated with EDTA for 30 min. Subsequently, EDTA was removed by buffer exchange with 10 mM MOPS (pH 7.0). The activity of this apoXI assayed in the absence of added bivalent metal ions was <0.02 unit/mg.

In most cases, XI activities were measured by a coupled enzyme assay using D-sorbitol dehydrogenase (SDH).[35] D-Xylulose formed by XI activity is reduced by SDH to xylitol, which is monitored by following NADH oxidation spectrophotometrically at 340 nm. SDH was obtained from Roche Diagnostics GmbH (Mannheim, Germany). The standard reactions were performed at 30 °C, and the mixtures contained 20 mM MOPS (pH 7.0), 1 mM bivalent metal ions, 150 mM D-xylose, 0.15 mM NADH, and 1 unit/mL SDH. Reactions were initiated by adding 0.05−0.2 μM apoXI. The amount of XI was adjusted so that the ratio of SDH activity to XI activity would be at least 30. In the case of assays in the presence of Co^{2+}, the amount of SDH was doubled to balance the inhibitory effect of Co^{2+} ions on SDH activity. The absorbance at 340 nm was followed using a spectrophotometer (Jasco) or a Synergy Mx microtiter plate reader (BioTek Instruments, Inc.). D-Xylose and D-fructose stocks (2 M) were made in Milli-Q water and stored at −20 °C. The measurements were performed in duplicate. One unit of XI activity is defined as the amount of enzyme catalyzing conversion of 1 μmol of D-xylose per minute under the assay conditions.

Kinetic parameters of XI for D-xylose were determined by measuring XI activity with varying D-xylose concentrations in the range of 0.04−1875 mM, depending on the metal cofactor used. For pH profiling of XI activities, different buffers (50 mM) were used to establish pH values: MES for pH 5.5 and 6.0 and MOPS for pH 6.5, 7.0, and 7.5. Activities of the native enzyme isolated from *E. coli* were measured in the presence of 1 mM $MgCl_2$ using the spectrophotometric assay described above. For determining the apparent metal affinities (K_{act} values), the activity of apo-PirXI was measured in the presence of varying metal concentrations (1−4000 μM) using 150 mM xylose as the substrate for Mg^{2+} and Mn^{2+}, 1375 mM xylose for Ca^{2+}, and 15 mM xylose for Co^{2+}. The concentration of the enzyme used was in the range of 0.05−0.2 μM for the reactions with Mg^{2+}, Mn^{2+}, and Co^{2+} and 0.5−1.0 μM for the reaction with Ca^{2+}.

For measuring the activities of PirXI with metal cofactors that are not compatible with the SDH-coupled assay, activities were examined by measuring the formation of D-xylulose from D-xylose by high-performance liquid chromatography (HPLC). Reaction mixtures containing the substrate, PirXI, and 1 mM metal ions in MOPS (pH 7.0) were incubated at 30 °C while being shaken. Reactions were stopped by acidification with HCl and addition of acetonitrile to a final concentration of 80%. Samples were then separated on an XBridge BEH Amide column (4.6 mm × 250 mm, pore size of 130 Å, particle size of 3.5 μm, Waters). Separation conditions were isocratic with 80% acetonitrile and 20% 20 mM MOPS (pH 7.0) and a flow rate of 1 mL/min at 80 °C. The ultraviolet (UV) absorbance at 210 nm was measured for D-xylulose quantification. For measuring XI activity with Fe^{2+}, oxygen-limited reaction mixtures were prepared by flushing the reaction components and the mixture with argon. The reaction mixtures were incubated in a 30 °C water bath. During the reaction, the argon was flushed over the surface of the reaction mixture, and for sampling, a syringe was used. The activity of PirXI on glucose was also measured using the HPLC assay as described above. The activities with different concentrations of glucose ranging from 0.1 to 1.5 M were measured in the presence of 1 mM $MgCl_2$ as the metal cofactor. A refractive index detector was employed for D-fructose quantification.

Metal Analysis. XI purified from *E. coli* was lyophilized and analyzed for the presence of calcium, cobalt, copper, iron, magnesium, manganese, and zinc using inductively coupled plasma optical emission atomic spectroscopy on an Optima 7000DV ICP-OES apparatus (PerkinElmer). The measurements were performed in duplicate. Before lyophilization, a molybdenum standard (molybdenum ICP standard Certipur, Merck Millipore) was added to the sample to a final concentration of 5.0 μg/mL.

Crystallization and Structure Determination. Initial vapor-diffusion crystallization experiments were performed using a Mosquito crystallization robot (TTP Labtech). In a typical experiment, 0.1 μL of the screening solution was added

DOI: 10.1021/acs.biochem.7b00777
Biochemistry 2017, 56, 5991−6005

Table 1. Data Collection and Refinement Statistics

	native	apo	Mg–glycerol	Mg–xylitol	Mg–xylose	Ca–xylose	Mn–xylose	Mn–sorbitol	Fe–glycerol	Co–xylulose	Ni–xylose	Cd–xylose
cryoprotectant	20% glycerol	20% glycerol	0.5 M xylose and 20% glycerol	2.2 M xylitol	2.2 M xylose	2.2 M xylose	2.2 M xylose	2.2 M sorbitol	20% glycerol	0.25 M xylulose and 2.5 M transPRO	2.2 M xylose	2.2 M xylose
unit cell dimensions												
a, *b*, *c* (Å)	78.7, 79.4, 92.2	78.9, 79.4, 91.1	78.6, 79.4, 92.1	78.8, 79.3, 91.8	78.6, 79.3, 92.0	78.8, 79.3, 91.9	78.7, 79.4, 92.1	79.0, 79.4, 91.3	79.5, 79.5, 92.2	79.3, 79.3, 91.4	78.2, 79.0, 92.0	78.6, 79.4, 92.0
α, β, γ (deg)	115.3, 90.3, 117.0	115.8, 89.4, 116.7	115.5, 90.2, 116.9	115.4, 90.2, 116.7	115.4, 89.9, 117.1	115.4, 89.9, 117.2	115.4, 90.0, 117.1	115.7, 89.4, 116.9	115.6, 90.0, 117.7	115.7, 89.4, 116.9	115.1, 90.4, 117.0	115.4, 90.0, 117.2
resolution (Å)	1.80	1.67	1.80	1.75	1.90	1.86	2.08	1.80	2.40	1.93	1.80	1.86
R_{sym} (%)[a]	4.5 (23.0)	7.8 (28.6)	8.9 (35.0)	6.6 (43.1)	9.3 (35.3)	9.0 (48.8)	11.0 (43.5)	9.4 (48.2)	13.9 (49.0)	7.8 (29.3)	8.8 (49.1)	6.3 (38.6)
completeness (%)[a]	92.3 (66.7)	92.4 (75.6)	93.4 (80.7)	93.3 (89.0)	92.0 (84.7)	93.7 (75.7)	92.4 (59.7)	93.6 (79.6)	85.8 (81.1)	94.3 (79.3)	91.4 (87.3)	87.8 (55.9)
$I/\sigma(I)$[a]	20.6 (4.9)	9.1 (3.7)	8.4 (2.6)	14.0 (2.9)	6.1 (2.0)	10.6 (2.1)	9.3 (2.7)	11.6 (2.1)	5.9 (2.1)	10.9 (2.9)	8.0 (1.9)	9.4 (2.0)
redundancy	3.9 (3.2)	4.0 (3.8)	4.0 (3.6)	4.0 (4.0)	2.0 (2.0)	4.0 (3.2)	3.9 (2.9)	3.9 (3.2)	4.0 (4.0)	2.8 (2.4)	3.8 (3.8)	2.0 (1.8)
						Refinement						
R/R_{free} (%)	12.1/14.8	18.4/21.0	19.4/22.9	14.0/16.1	15.3/17.6	17.6/20.1	16.8/20.3	15.5/18.1	24.4/27.8	15.7/18.8	15.4/17.5	14.4/16.5
ions for active site occupancy	4 (Ca^{2+}, Mg^{2+}, Fe^{2+}) 0.4, 0.35, 0.25	–	4 Mg^{2+}	4 Mg^{2+}	8 Mg^{2+} in two conformations	8 Ca^{2+}	8 Mn^{2+}	8 Mn^{2+}	8 Fe^{2+}	8 Co^{2+} in two conformations	8 Ni^{2+} in two conformations	8 Cd^{2+}
ligand active site	glycerol	glycerol	glycerol	xylitol	linear xylose	linear xylose	linear xylose	sorbitol	–	xylulose	linear xylose	linear xylose or xylopyranose
waters	2373	2317	1638	1836	1775	1620	1522	1984	477	2185	1751	1837
other ligands				–	14 xylose	8 xylose	8 xylose	–	–	4-hydroxyproline	15 xylose	13 xylose
other atoms	20 GOL, 3 SO_4^{2-}	7 GOL, 4 SO_4^{2-}, 2 acetate	11 GOL, 3 SO_4^{2-}	3 SO_4^{2-}	7 SO_4^{2-}	6 SO_4^{2-}, 2 Ca^{2+}	3 SO_4^{2-}	4 SO_4^{2-}	3 SO_4^{2-}	–	5 SO_4^{2-}	8 SO_4^{2-}
root-mean-square deviation												
bond lengths (Å)	0.013	0.009	0.014	0.010	0.010	0.009	0.012	0.012	0.012	0.011	0.011	0.011
bond angles (deg)	1.49	1.31	1.48	1.33	1.32	1.24	1.37	1.48	1.42	1.38	1.37	1.42
PDB entry	5NH5	5NHM	5NH4	5NH6	5NH7	5NH8	5NH9	5NHA	5NHB	5NHC	5NHD	5NHE

[a]Values in parentheses are for the highest-resolution shell.

DOI: 10.1021/acs.biochem.7b00777
Biochemistry 2017, 56, 5991–6005

Table 2. Metal Dependence of PirXI Activity[a]

substrate	cation	V (200 mM) (s^{-1})	k_{cat} (s^{-1})	K_M (mM)	k_{cat}/K_M (s^{-1} M^{-1})	K_{act}[c] (μM)
xylose	Mg^{2+}	1.95 ± 0.12[b]	2.0 ± 0.1	7.5 ± 1.2	270	98.9 ± 4.3
xylose	Mn^{2+}	4.4 ± 0.42[b]	4.5 ± 0.3	4.3 ± 0.1	1100	1.45 ± 0.28
xylose	Ca^{2+}	0.075 ± 0.017[b]	0.8 ± 0.1	1930 ± 70	0.2	159 ± 10
xylose	Co^{2+}	1.0 ± 0.14[b]	1.0 ± 0.1	0.3 ± 0.04	3300	6.5 ± 1.21
glucose	Mg^{2+}	0.032 ± 0.005[b]	0.1 ± 0.01	430 ± 10	0.2	–
xylose	Zn^{2+}	1.1 ± 0.1	–	–	–	–
xylose	Fe^{2+}	1.6 ± 0.2	–	–	–	–
xylose	Cd^{2+}	0.2 ± 0.01	–	–	–	–
xylose	Ni^{2+}	nd[d]	–	–	–	–
xylose	Al^{3+}	nd[d]	–	–	–	–

[a]The values represent averages and the mean deviation calculated from two or three replicates. [b]Initial rates at 200 mM substrate were calculated from steady state parameters. [c]K_{act} is defined as the metal concentration at which the enzyme activity is half the V_{max}. [d]No activity detected with the HPLC assay described in Materials and Methods.

to 0.1 μL of the protein solution on a 96-well MRC2 plate (Molecular Dimensions); reservoir wells contained 50 μL of the screening solution. The screening solutions used for the experiments were PACT and JCSG+ (Qiagen Systems). Crystallization conditions were optimized using hanging-drop setups with 13−15% (w/v) PEG 3350 and 0.1 M ammonium sulfate in 0.1 M HEPES (pH 7.0) as a precipitant, and drops containing 1 μL of the protein solution [6 mg mL^{-1} in 10 mM triethanolamine (pH 7.6)] and 1 μL of the reservoir solution at 295 K. Native PirXI crystals belong to space group $P1$ with four 49 kDa monomers in the asymmetric unit. The V_M is 2.3 $Å^3$/Da[36] with a solvent content of 45%. Apo crystals were grown under the same condition as native crystals, and binary complexes of apo-XI with metal cofactors were prepared by addition of the required metal in the crystallization drop. Before data collection, crystals were briefly soaked in a cryoprotectant solution, consisting of 20% glycerol, 15% (v/v) PEG 3350, and 0.1 M ammonium sulfate in 0.1 M HEPES buffer (pH 7.0). Ternary complexes with substrate or inhibitor were prepared from the binary complexes by stepwise addition of the sugars to the crystals, reaching a final sugar concentration of 2.2 M, which was high enough for the sugar to serve as a cryoprotectant.[37] For the structure of XI with xylulose, 2.5 M *trans*-4-hydroxy-L-proline was used as a cryoprotectant as xylulose was available only as a 0.5 M solution.

X-ray diffraction data to 1.8 Å resolution were collected from single cryo-cooled crystals mounted on an in-house MarDTB Goniostat System using Cu Kα radiation from a Bruker MicrostarH rotating-anode generator equipped with HeliosMX mirrors. Intensity data were processed using iMosflm[38] and scaled using Aimless.[39]

Phases were obtained by molecular replacement using Phaser.[40] The coordinates of three xylose isomerase structures [Protein Data Bank (PDB) entries 1A0C, 1A0D, and 1A0E], which have sequences that are ∼50% identical with that of PirXI, were used to construct a composite search model. The PirXI structure was built using ArpWarp[41] and Coot[42] and refined using Refmac5.[43] Water molecules were placed automatically in $F_o - F_c$ difference Fourier maps at a 3σ cutoff level and validated to ensure correct coordination geometries using Coot. The first residues from the four XI subunits were not visible in the electron density and therefore not included in the final model. In the binary and ternary complexes, $2F_o - F_c$ and $F_o - F_c$ maps showed extra density in the active site. To confirm the metal ions, we calculated anomalous difference Fourier maps, with data collected at a wavelength of 1.54 Å (1.3 anomalous electrons for Ca, 2.8 for Mn, 3.2 for Fe, 3.7 for Co, 0.5 for Ni, and 4.7 for Cd), using phases obtained from the model without any metal ions. Occupancies of the metal ions were calculated with Phenix.[44] Relevant statistics of data collection and model refinement are listed in Table 1. The stereochemical quality of the model was assessed with MolProbity.[45] Interface areas between the subunits were calculated with PDBePISA.[46] Figures were prepared with PyMOL (http://www.pymol.org) and ESPript.[47] Atomic coordinates and experimental structure factor amplitudes have been deposited in the PDB (Table 1).

Structure-Based Sequence Alignment. A structure-based alignment of class II xylose isomerases from *Piromyces* sp. E2, *Bacteroides thetaiotaomicron* (PDB entry 4XKM),[34] *Thermoanaerobacterium thermosulfurigenes* (PDB entry 1A0C), *Thermotoga neapolitana* (PDB entry 1A0E), and *Bacillus stearothermophilus* (PDB entry 1A0D) and a class I xylose isomerase from *St. rubiginosus* (PDB entry 4W4Q)[48] was made with Promals3D.[49] The alignment figure was created with ESPript.[50]

RESULTS

Expression of PirXI in *E. coli* and Enzyme Isolation. To overexpress the *Piromyces* sp. E2 xylose isomerase (PirXI) in *E. coli*, a codon-optimized synthetic *xylA* gene was cloned into the pBAD vector and transformed into *E. coli* Top10. Overnight cultivation at 37 °C with induction of expression of PirXI by 0.2% arabinose resulted in high levels of soluble PirXI. Sodium dodecyl sulfate−polyacrylamide gel electrophoresis (SDS−PAGE) analysis showed that PirXI is the predominant protein in cell lysates, accounting for >50% of the total soluble protein. This allowed purification by a single step of ion-exchange chromatography, which after desalting routinely yielded 300−500 mg of purified xylose isomerase per liter of culture. From this material, the apoenzyme was prepared by treatment with EDTA to study the metal dependence of the isomerase activity. The purified enzyme was stored at −80 °C for use in further biochemical experiments.

SDS−PAGE showed that the size of the protein monomer is around 50 kDa, which is in good agreement with the calculated size of the protein, 49.5 kDa. Analytical size exclusion chromatography revealed a molecular weight of ∼200 kDa for the native PirXI, showing that the enzyme is a tetramer.

Metal Dependence of PirXI Activity. Because xylose and glucose isomerases require bivalent metals for activity[51] and the type of metal that is bound may influence the activity,[28] we

DOI: 10.1021/acs.biochem.7b00777
Biochemistry 2017, 56, 5991−6005

examined the effect of different metal ions on the activity of PirXI. Kinetic parameters of apo-PirXI in the presence of Mg^{2+}, Mn^{2+}, Co^{2+}, or Ca^{2+} were measured using the SDH-coupled assay as described in Materials and Methods.

PirXI showed good activity in the presence of Mg^{2+}, Co^{2+}, and Mn^{2+} (Table 2). Among these metals, the highest activity (k_{cat}) of the enzyme was obtained with Mn^{2+}, followed by Mg^{2+} and Co^{2+}. The substrate affinity with xylose (K_M), on the other hand, was best in the presence of Co^{2+}, which gave a K_M of 0.3 mM and also the highest catalytic efficiency (k_{cat}/K_M). In the presence of Mn^{2+} or Mg^{2+}, the K_M of the enzyme was 15−20-fold higher. This metal preference of PirXI is similar to what was described for other class II XIs, which were reported to be most active with Mn^{2+}, whereas the class I enzymes are most active with Mg^{2+}.[28,31,32] When Ca^{2+} was added as the metal cofactor of PirXI, the enzyme showed activity, although it was lower than with the other metals mentioned above. A striking observation was the extremely low xylose affinity ($K_M \sim 2$ M) in the presence of Ca^{2+}, resulting in a poor catalytic efficiency ($k_{cat}/K_M = 0.2\ s^{-1}\ M^{-1}$). The low substrate affinity suggests that the Ca^{2+}-containing enzyme will provide a negligible contribution to *in vivo* conversion of xylose by PirXI.

Further assays for determining the metal dependence of PirXI activity were performed using an HPLC assay for measuring xylulose formation because the SDH-coupled assay is not compatible with the presence of Zn^{2+}, Fe^{2+}, Cd^{2+}, Ni^{2+}, and Al^{3+} as these metals inhibit SDH activity. Furthermore, in the case of Fe^{2+}-dependent activity, the reactions were performed under reduced oxygen conditions to prevent oxidation of Fe^{2+} to Fe^{3+}. In these experiments, we measured initial conversion rates (units per milligram) of xylose that was added to a final concentration of 200 mM. PirXI showed activity in D-xylose isomerization in the presence of Zn^{2+}, Fe^{2+}, and Cd^{2+}. The rate of xylose conversion with Zn^{2+} was almost half of that measured with Mg^{2+}. Furthermore, Fe^{2+} gave moderate activity compared to activities with other metals. Unexpectedly, the enzyme also showed some activity in the presence of Cd^{2+}, which was reported to be an inhibitor of another xylose isomerase.[26] However, the activity (0.2 unit/mg) was very low. No detectable amount of xylulose (<50 μM) was found with Ni^{2+} or Al^{3+} as the metal cofactor upon measurement after incubation of the reaction mixture for 2 h.

Metal Affinity of PirXI. The results described above show that PirXI can be activated by a range of different bivalent metal ions. Obviously, the activity *in vivo* will also be determined by metal affinity and metal availability in the cytoplasmic environment. Therefore, we investigated the activity of PirXI on xylose in the presence of different concentrations of divalent metals and determined half-saturation constants for activation of the enzyme [K_{act} values (Table 2)].

Of the metals tested (Mg^{2+}, Mn^{2+}, Co^{2+}, and Ca^{2+}), the highest affinity was found with Mn^{2+}. The enzyme also showed a high affinity for cobalt, but the affinities for Mg^{2+} and Ca^{2+} were 70- and 100-fold lower compared to that of Mn^{2+}, respectively.

Analysis by inductively coupled plasma atomic emission spectroscopy showed that the main divalent metal in native PirXI isolated from *E. coli* is Mg^{2+}, which accounted for approximately half of the total metal content (Table 3). Ca^{2+} and Fe^{2+} were also detected, whereas the enzyme contained only a few percent (moles per mole) of Mn^{2+} and Zn^{2+}. This indicates that Mg^{2+} would strongly influence the *in vivo* enzyme activity in *E. coli*, while Mn^{2+} ions, which are most beneficial for activity, would have little influence. In agreement with this, the native enzyme isolated from *E. coli* showed activity similar to that of the enzyme reconstituted with Mg^{2+} or even slightly lower activity, probably due to the effect of Ca^{2+} and Fe^{2+}. The metal composition and the activity of the enzyme are slightly different from one batch of isolated enzyme to another (WT1−WT3). The data also suggest that intracellular metal availability influences the metal composition of the enzyme (Mg > Ca > Mn > Co) as much as the relative affinities (Mn > Co > Mg > Ca). Accordingly, *in vivo*, the enzyme may have suboptimal activity because of the level and type of metal binding. Recently, Verhoeven et al.[33] showed that the increase in the intracellular Mn^{2+} level improved the growth of *S. cerevisiae* on xylose by enhancing PirXI activity.

Table 3. Metal Contents of PirXI Purified from *E. coli*[a]

	mol of metal/mol of PirXI						nXI activity
	Ca	Fe	Mg	Zn	Co	Mn	k_{obs} (s^{-1})
WT1	0.59	0.35	1	0.03	*b*	0.01	1.9 ± 0.1
WT2	0.7	0.4	0.93	0.03	*b*	0.01	1.7 ± 0.03
WT3	0.56	0.36	1.28	0.02	*b*	0.02	2.1 ± 0.06

[a]The metal content of PirXI purified from *E. coli* was measured, and the moles of metal per mole of enzyme monomer were calculated. WT1−WT3 represent the enzyme purified from three independent cultures. The activities of the holoenzymes were measured with 150 mM xylose. The indicated k_{obs} values are averages and mean deviations of duplicate measurements. [b]Below the detection limit (<0.002 mol/mol of PirXI).

pH Dependence of PirXI Activity. The cytosolic pH of *S. cerevisiae* during the fermentation process is <7.0, possibly because of the influence of acidic lignocellulose hydrolysate.[52,53] We measured the activity of PirXI at different pH values ranging from 5.5 to 7.5 in the presence of Mg^{2+}, Mn^{2+}, Ca^{2+}, or Co^{2+} (Figure 2). Because of the high K_M of the enzyme in the presence of Ca^{2+}, the activity was measured at a higher xylose concentration, 1 M instead of 150 mM. With Mg^{2+}, Mn^{2+}, and Ca^{2+}, the results show a similar broad pH profile, with the highest activity at pH 7.5, and a significantly reduced activity at pH 6.5. The lower activity at low pH was more pronounced for Mg^{2+}, the quantitatively most important cation in the non-reconstituted enzyme. The activity of the Co^{2+}-reconstituted PirXI was much less dependent on pH in the range of 5.5−7.5.

Crystal Structure of PirXI. PirXI isolated from *E. coli* readily crystallized from PEG 3350 at pH 7. The structure was determined by using X-ray diffraction and molecular replacement and was refined against 1.8 Å resolution diffraction data to an R factor of 0.116 (R_{free} = 0.148) with good stereochemistry (Table 1 and Figure 3A). The P1 unit cell contains four monomers that form a 92 Å × 77 Å × 77 Å tetramer, having noncrystallographic 222 symmetry. The four subunits have root-mean-square deviation (rmsd) values of 0.11−0.16 Å on Cα atoms. Each PirXI subunit comprises two structural domains, a larger catalytic domain (residues 1−377) with a distorted $(\beta/\alpha)_8$-barrel (TIM-barrel) fold and a C-terminal domain (residues 378−437) forming an extended tail containing three α-helices.

With other class II xylose isomerases with PDB entries of 4XKM (*B. thetaiotaomicron*),[34] 1A0C (*T. thermosulfurigenes*), 1A0D (*B. stearothermophilus*), and 1A0E (*Th. neapolitana*), rmsd values are 0.4 Å on 435 Cα atoms, 1.2 Å on 430 Cα atoms, 1.1 Å on 425 Cα atoms, and 1.2 Å on 422 Cα atoms,

DOI: 10.1021/acs.biochem.7b00777
Biochemistry 2017, 56, 5991−6005

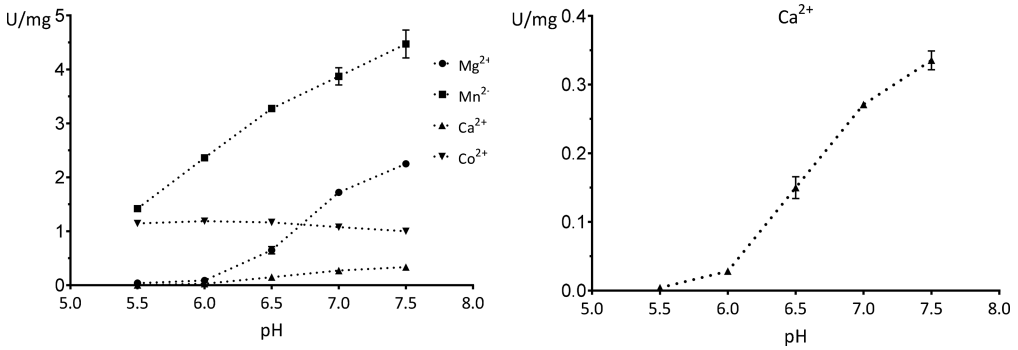

Figure 2. pH–activity profiles of PirXI in the presence of different metal cofactors. Specific activities (micromoles per minute per milligram) of PirXI on xylose (150 mM for Mg^{2+}, Mn^{2+}, and Co^{2+} and 1 M for Ca^{2+}) were measured at various pH values in the presence of different metal ion cofactors. The error bars indicate the mean deviations of duplicate measurements.

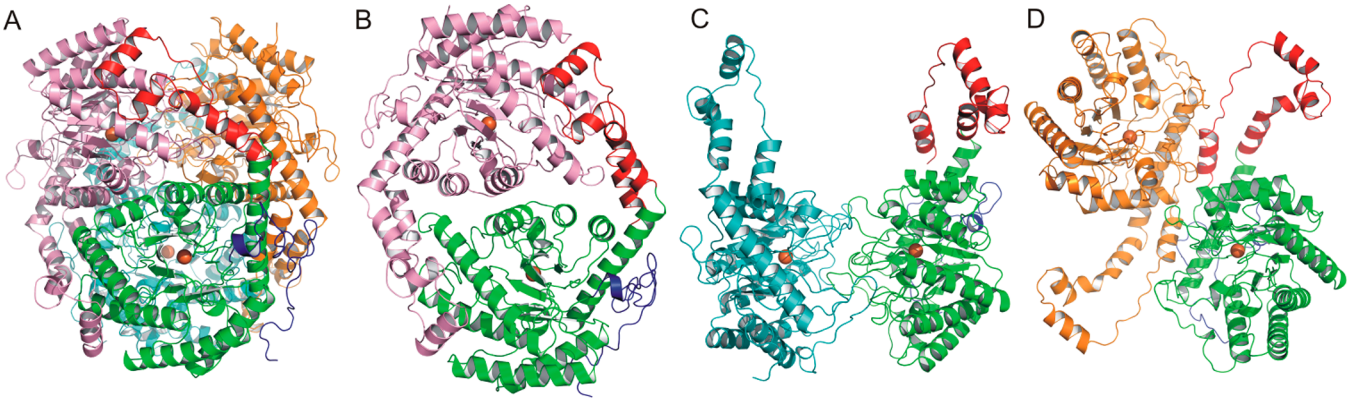

Figure 3. Overall crystal structure of PirXI. PirXI is displayed in cartoon format, and subunits B–D are colored pink, cyan, and orange, respectively. The catalytic domain of subunit A is colored green, the N-terminal extension dark blue, and the C-terminal domain red. Ions at position M1 are colored orange. (A) Tetramer and possible dimer pairs in (B) the yin-yang dimer (subunits A and B), (C) the butterfly dimer (subunits A and C), and (D) the diagonal dimer (subunits A and D).

respectively, while with the well-studied *St. rubiginosus* class I enzyme, the rmsd is 2.0 Å on 352 Cα atoms and 27% sequence identity. Major differences between the class I *St. rubiginosus* XI and the class II PirXI are the presence in the latter enzyme of an N-terminal extension of ~33 residues, an N-terminal addition of α-helix 1, and a larger loop before α-helix 2. Furthermore, the C-terminal regions deviate the most with low identity, except for the ultimate α-helix 12 (Figure S1).

A pair of subunits forms the "yin-yang" dimer with rotational symmetry by contacts of the catalytic domain of subunit A interacting with the C-terminal tail of subunit B, while the core of subunit B is interacting with the C-terminal tail of subunit A (Figure 3B). The other dimer pairs are called the "butterfly" dimer (Figure 3C) and the "diagonal" dimer (Figure 3D). The tetramer has a surface area of 53920 Å^2, of which 36840 Å^2 is buried. Each subunit has a total solvent accessible surface area of 21100 Å^2, of which 8110 Å^2 is buried. The interactions in the yin-yang and diagonal dimers are mainly present between the N- and C-terminal tails of the subunits, while the butterfly dimer has interactions between the cores of the subunits.

The sizes of the interface areas are similar in other class II xylose isomerases for which the structures have been determined (PDB entries 4XKM, 1A0C, 1A0D, and 1A0E) (Table 4). However, the xylose isomerase from *St. rubiginosus*, the most studied class I XI in the PDB, has a larger interface for the yin-yang dimer (4670 Å^2) and a smaller interface for the diagonal dimer (1460 Å^2) as it is missing the N-terminal extension of the class II enzymes. Class II enzymes, having larger dimer interfaces and interactions with the other subunit, should be regarded as tetramers unlike class I enzymes, which are usually described as a dimer of dimers.[34]

Table 4. Subunit Organization of PirXI

	subunits	interface area (Å^2)	complexation significance score	no. of H-bonds/ salt bridges
tetramer	ABCD			
yin-yang	AB and CD	4050	0.505	51/28
butterfly	AC and BD	1395	0.210	22/12
diagonal	AD and BC	1823	0.233	27/14

Active Site Structure. The active sites of the PirXI subunits are located on the C-terminal end of the $(\beta/\alpha)_8$-barrel of the core domain. The active sites are 36 Å apart in yin-yang, 31 Å apart in butterfly, and 39 Å apart in diagonal dimers. Residues from the loops following the β-strands shape the active site. The active site pocket is lined by the side chain indole groups from Trp50 and Trp189 that are situated 8.8 Å from each other forming a cassette for sugar binding (Figure 4A,B). Other hydrophobic residues surrounding the substrate binding site are Phe61 from another subunit of the butterfly dimer, Phe146 and Trp140.

In the crystals obtained with native PirXI isolated from *E. coli*, only the position of the structural metal (M1) in the active site is occupied. Residues Glu233, Glu269, Asp297, and Asp340

DOI: 10.1021/acs.biochem.7b00777
Biochemistry 2017, 56, 5991–6005

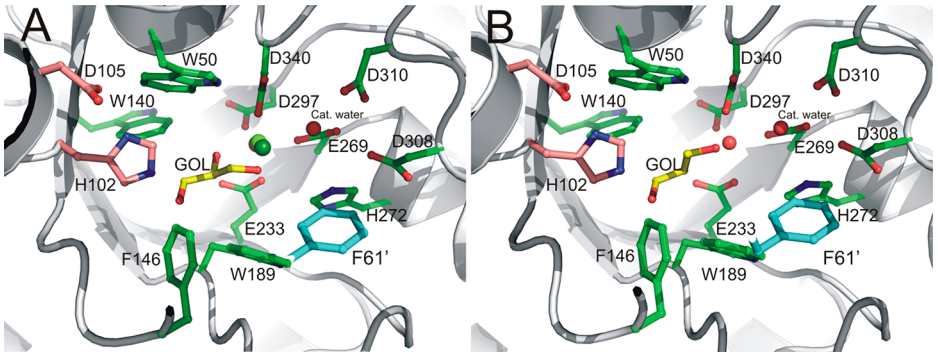

Figure 4. Active site of (A) native XI and (B) apo-XI. The residues forming the active site are shown as green sticks; the His102-Asp105 pair is colored salmon, and F61′ from another subunit is colored cyan and the glycerol molecule yellow. Water molecules are colored red. Ca^{2+} is colored dark green. Mg^{2+} is colored light green. Fe^{2+} is shown as brown spheres. Fe^{2+} is only slightly visible because of the overlapped position with Mg^{2+}.

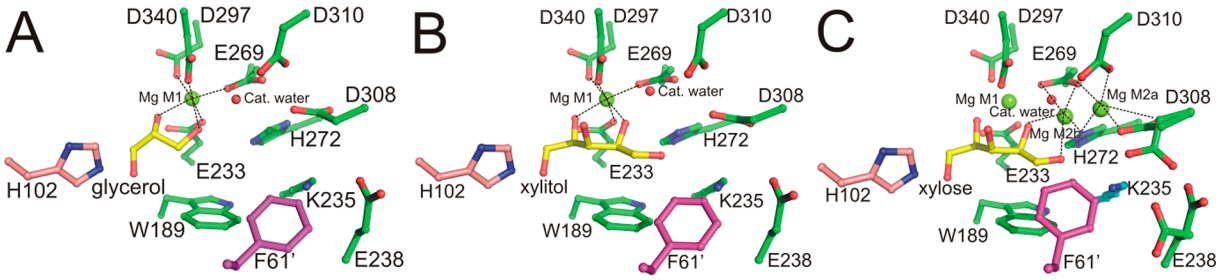

Figure 5. Active site of (A) Mg−GOL−XI, (B) Mg−XYL−XI, and (C) Mg−XLS−XI. The residues involved in metal binding are shown as green sticks. His102 is colored salmon. F61′ from another subunit is colored magenta. The glycerol, xylitol, and xylose molecules are colored yellow. Water molecules are shown as red spheres and Mg^{2+} ions as light green spheres.

bind M1 with octahedral geometry (Figure 4A). The nature of the metal ion was unclear from the structure as a mixture of different metals may bind. The observed metal−donor distances were 2.1−2.2 Å. The optimal distance for Ca^{2+} is 2.36 Å, for Mg^{2+} 2.26 Å, and for Fe^{2+} 2.01 Å to monodentate Asp or Glu.[54] An anomalous difference map showed a peak at the M1 position indicating a bound Ca^{2+} or Fe^{2+} ion. Refining with a Ca^{2+} ion with full occupancy showed residual $F_o - F_c$ density and distances that were too short, while refining with 100% Fe^{2+} showed deficit density and distances that were too long. Therefore, M1 was refined to occupancies of 0.4, 0.35, and 0.25 for Ca, Mg, and Fe, respectively, which gave a flat $F_o - F_c$ map after refinement. The ambiguous metal ion content has also been observed in native crystals of *St. rubiginosus* with 0.6 equiv of Mn, <0.6 equiv of Mg, and <0.1 equiv of Co per monomer.[55] In this PirXI structure, a glycerol molecule from the cryoprotectant is bound in the active site to the metal ion with a Me−O2 distance of 2.3 Å and a Me−O3 distance of 2.4 Å. Glycerol, acting as a sugar mimic, is often found in active sites of carbohydrate-converting enzymes.[56]

The crystal structure obtained with EDTA-treated XI is highly similar to the native structure with an rmsd of 0.1 Å. As expected, this apoenzyme does not contain any metals in the active site, but a glycerol molecule is bound as in the native enzyme. A water molecule is located at position M1; consequently, O3 of the glycerol has shifted 1.4 Å toward His272 (Figure 4B).

To determine if and how other metals bind to PirXI, crystal soaks were performed. Several structures of binary and ternary complexes of PirXI with metals, substrates, and inhibitors were determined (Table 1 and Table S1).

Mg, Xylose, and Xylitol Binding. In electron density maps of crystals of the apoenzyme soaked with magnesium and glycerol or with magnesium and the competitive inhibitor (or substrate analogue) xylitol,[28] only a single Mg^{2+} ion at the M1 site was observed (Figure 5A,B). There was no $2F_o - F_c$ density present for the Mg^{2+} ion at position M2, despite the presence of Mg^{2+} in the soak solution at 10 mM (Figure S2). Glycerol was bound as in the native PirXI crystals. The position of xylitol was overlapping with that of the glycerol molecule in the Mg−glycerol structure, but the larger xylitol molecule bound deeper in the active site toward the putative M2 position. Xylitol was bound with its O1 atom bound to NE2 of His272 and a water molecule, O2 to Glu233, Glu269, Asp340, and M1 (Mg^{2+}), O3 to Asp340 and a water molecule, O4 to Glu233 (bidentate), Asp297, Asp340, and M1, and O5 to NE2 of His102 and a water molecule (Figure 5B). His102 is likely involved in pyranose ring opening.[26,57]

Only when a soak was performed with magnesium and the substrate D-xylose was the second metal site (M2) fully occupied with elongated (elliptical) electron density, showing two distinct positions for the metal, with approximately 50/50 occupancy, at distances of 3.8 Å (M2b) and 5.5 Å (M2a) from M1 (Figure 5C). It has been elucidated by structural studies, including neutron diffraction, that the hydride shift of the isomerization reaction is mediated by the metal at M2.[25,26,58,59]

In the Mg−xylose structure, the substrate is in its open form in the same conformation as xylitol, indicating ring opening has been completed. At the current resolution of the data sets (1.9 Å), it is not possible to distinguish between the linear forms of the substrate and product by electron density, and probably a mixture of both is bound. The open chain forms are similar in shape, and differences exist at only C1 and C2, having sp^2 or sp^3

DOI: 10.1021/acs.biochem.7b00777
Biochemistry 2017, 56, 5991−6005

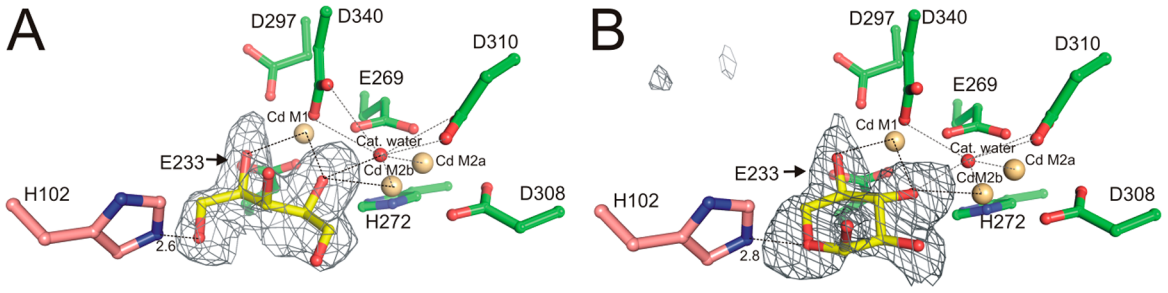

Figure 6. Active sites of (A) Cd–linear XLS–XI and (B) Cd–cyclic XLS–XI. The residues involved in the metal binding sites are shown as green sticks. His102 is colored salmon. The xylose molecules are colored yellow. Cd^{2+} ions are depicted as light orange spheres, and interactions between the metal ions and the hydroxyl groups of xylose or the protein environment are shown as dashed lines. The difference electron density, $F_o - F_c$, contoured at the 2σ level for the sugars is shown.

hybridization. Because all soaks were performed with a high concentration (2.2 M) of substrate and the rate-limiting step in the catalytic cycle was proposed to be the hydride-shift reaction,[30,60] we have modeled the substrate used in the soak. The xylose stacks on the ring system of Trp189, which probably ensures a flat conformation of the substrate (Figure 5C). The M2b metal has interactions with O1 and O2 of the xylose, NE2 of His272, Glu269 (bidentate), and a water molecule. The metal at M2b is in the catalytically more favorable position as the interactions with O1 and O2 likely stabilize the transition state while the hydride is shifting from C2 to C1. These interactions with O1 and O2 of xylose are absent when the metal is at position M2a. It was therefore suggested that the metal moves from position M2a to position M2b during the reaction.[25] Mg^{2+} at M2a is 2.0 Å from M2b and has interactions with NE2 of His272, OE2 of Glu269, OD1 of Asp310, Asp308 (bidentate) in one of its conformations, and the water molecule. In another conformation, Asp308 and O1 of the xylose have interactions with NZ of Lys235, which has moved closer into the active site compared to its position in the Mg–xylitol structure (Figure 5C). Glu238, having a H-bond with the backbone amide of Asp308, also has achieved a double conformation. Hence, its structural neighbor, the side chain of Phe61 from the adjacent subunit, shifts by 1.4 Å toward the substrate. The double side chain conformations of Asp308 and Glu238, obtained upon binding of the catalytic Mg^{2+} ion and xylose, are also observed in *St. rubiginosus* XI with two Mg^{2+} atoms and xylitol/xylose in the active site and *Arthrobacter* XI.[55,61] The conformational changes of the residues appear to be a consequence of the movement of the metal from M2b to M2a as it causes the aspartate to lose its coordination with the metal and interact with the nearby glutamate.

XI–Cd and XI–Mn–Sorbitol. In the Cd–xylose complex of PirXI, bound substrates are in a linear form (XLS) in subunit A and subunit B, while in subunit C and subunit D of the yin-yang dimer, the substrates are in the pyranose ring form (Figure 6A,B). This mixture of open and closed structures was observed for only the PirXI–Cd structure. For PirXI structures soaked with other metals, the electron density map showed only the linear form of the substrate in the active site (Figure S2B–D). The active site structure of PirXI–Cd with the xylose in a linear form is very similar to the structure of Mg–xylose. Cd^{2+} at M2 is observed at two distinct positions with a 1.4 Å distance between M2a and M2b.

The electron density map in the active centers of subunits C and D shows α-D-xylopyranose (XYS) that is coordinated to M1 with O3 and O4, whereas endocyclic O5 is hydrogen bonded to His102. O4 of α-D-xylopyranose is also coordinated to M2b at a distance of 2.7 Å (Figure 6B).

The crystal structure of XI–Mn soaked with sorbitol, a C6 sugar analogue with the same stereo configuration as D-glucose, shows two singly occupied metal binding sites (Figure 7). The

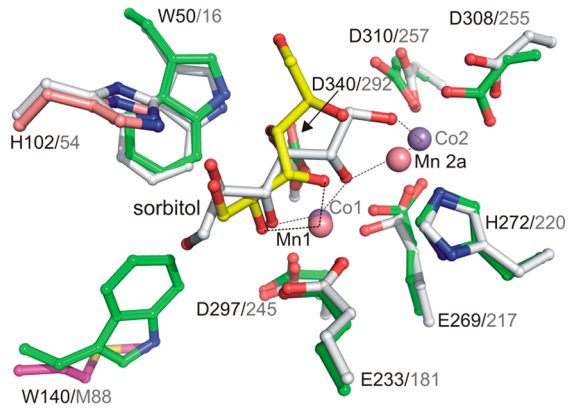

Figure 7. Overlay of the active sites of Mn–SOR–XI and XI from *A. missouriensis* complexed with Co^{2+} and sorbitol (PDB entry 2XIN). The residues involved in the metal binding sites are shown as green sticks. His102 is colored salmon. The sorbitol molecule is colored yellow. The residues and sorbitol from 2XIN are colored gray. Mn^{2+} ions are shown as purple spheres and Co^{2+} ions as pink spheres. Interactions between the metal ions and hydroxyls of the sorbitol are shown as dashed lines.

binding of the sorbitol is quite different from the binding of xylitol in the Mg–xylitol structure. O1 of sorbitol interacts with His102 (2.6 Å) and a water molecule, and O2 interacts with Glu233 (bidentate), Asp297, and M1-Mn^{2+}. O3 is ligated by Glu233, Asp340, and M1, and O4 is ligated by Asp340 (bidentate) and Ne of Trp50. O5 and O6 have interactions with water molecules. Interactions with M2 occur via water molecules. The binding mode of sorbitol is also quite different from that in class I XI from *A. missouriensis* complexed with Co^{2+} and sorbitol (Figure 7) and from *St. rubiginosus* complexed with Ni^{2+} and sorbitol.[62,63] In class II enzymes, the bulkier Trp140 replaces a Met (Figure S1) in the rear side of the active site. Therefore, steric hindrance was expected in the active site of class II XI as the C6 atom of sorbitol would be too close to Trp140. In PirXI, the sorbitol molecule has shifted by 2.3 Å toward the entrance of the active site. Assuming that its C6 analogue binds in a similar manner, we found that glucose would bind to the active site in a less productive mode.

DOI: 10.1021/acs.biochem.7b00777
Biochemistry 2017, 56, 5991–6005

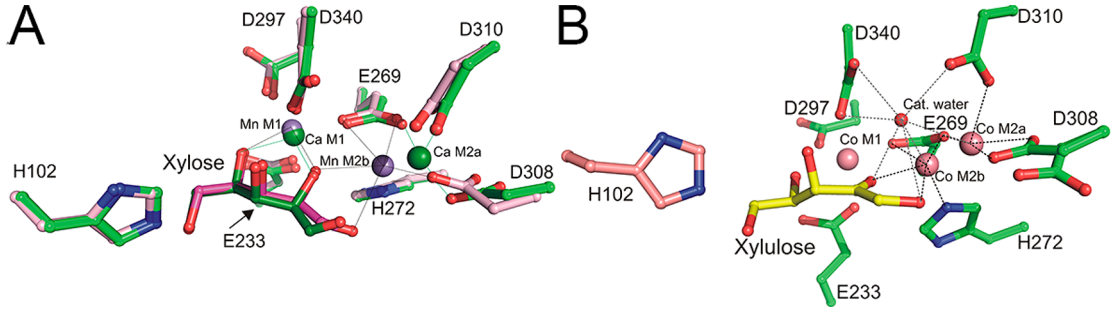

Figure 8. Overlay of the active sites of Mn−XLS−XI and Ca−XLS−XI (A) and the active site of Co−XUL−XI (B). In panel A, the residues involved in calcium binding are shown as green sticks. The bound manganese is colored pink. The xylose molecule in the Ca^{2+} structure is colored forest green and in the Mn^{2+} structure magenta. In panel B, the residues involved in the metal binding sites are shown as green sticks. His102 is colored salmon. The xylose molecules are colored yellow. Co^{2+} ions are colored pink. Interactions between the metal ions and the ligand amino acids and hydroxyl of the xylose/xylulose are shown as dashed lines (green for Ca^{2+} and black for Mn^{2+} in panel A).

XI−Ni, XI−Fe, and XI−Ca. The XI−Fe structure contains two iron atoms in the active site 1.9−2.2 Å from the surrounding ligands (Figure S3A). No glycerol molecules could be observed in the electron density, which could be caused by the lower resolution of the data set. The M2 Fe^{2+} is positioned at the M2b location 2.4 Å from His272. The Fe^{2+} atoms are positioned 3.8 Å from each other.

A soak with xylose of a Ni^{2+}-grown XI crystal reveals xylose in its linear form in the active site (Figure S3B). Its position superimposes well on the Mg−xylose structure. The Ni^{2+} cation at position M2 has two distinct locations (M2a and M2b), as in the Mg−xylose structure. However, Asp308 does not have the double conformation as observed in the Mg−xylose structure.

A soak with Ca^{2+} resulted in both positions M1 and M2 being occupied (Figure 8A). M2 is bound in a distorted octahedral geometry by His272 at 3.4 Å, Glu269 at 2.3 Å, Asp308 at 2.2 Å, Asp310 at 2.4 Å, and two water molecules. To the best of our knowledge in Class I XIs, the M1 site was never occupied by a Ca^{2+} ion. At M2, other class I XIs bound Ca^{2+} at the M2a position, similar to what we observed in the PirXI−Ca^{2+}−xylose structure, but the equivalent residue of Asp308 binds the M2 in a bidentate manner in other enzymes.[48] The large size of M2−Ca^{2+} shifts Asp308 and Asp310 slightly out and the O1 position of the linear xylose by 1.5 Å toward Phe61′. This leaves the substrate in an unfavorable position for isomerization.

XI−Mn, XI−Co, and XI Substrate/Product. The PirXI structure with two manganese ions and the substrate xylose well represents the most active form of the enzyme (Figure 8A). The Mn^{2+} at position M1 has its usual octahedral coordination, while M2 has full occupancy at the catalytic M2b position (no occupation of the M2a site). The M1 and M2b metal binding sites are 4.1 Å distance from each other. M2b is coordinated by His272 at 2.4 Å, Glu269 at 2.3 and 2.9 Å, Asp308 at 2.0 Å, Asp310 at 3.2 Å, and O1 of xylose at 2.8 Å and O2 at 2.7 Å. The coordination is highly similar to that observed in the *A. missouriensis* XI (9XIM) mutant E186Q ternary complex with two Mn^{2+} atoms and a linear xylose.[62] It is interesting that in the PirXI structure with the highest activity, which is the Mn^{2+}-dependent activity (Table 2), only the M1 and M2b sites are occupied, not M2a.

Xylulose was soaked in a Co^{2+} cocrystallized crystal and cryoprotected with 2 M proline. The structure showed that M2-Co^{2+} ion occupies two positions (M2a and M2b) with a 1.8 Å distance (Figure 8B). Furthermore, similar conformational changes for Asp308, Asp310, and Phe61′ are observed as in the Mg^{2+}−xylose structure. In this structure, we modeled D-xylulose as it was present at a concentration of ∼0.25 M in the soaking solution. The position is similar to that of the xylulose found in the crystal structure of *St. rubiginosus* (1XII)[64] and in the neutron diffraction structure of *St. rubiginosus* (3XWH).[57]

DISCUSSION

An efficient xylose isomerase that is well expressed in the active form in *S. cerevisiae* is critically important for the development of xylose-fermenting yeast strains. The *Piromyces* sp. E2 xylose isomerase has emerged as an attractive enzyme for this purpose.[5] Our recent work indicates that metal incorporation is critical for *in vivo* activity, as suggested by the effect of mutations influencing manganese homeostasis on XI activity and anaerobic xylose metabolism.[33] Our work corroborates this by exploring the metal dependence of the catalytic performance and by examining crystal structures of the enzyme soaked with different metals, substrates, and substrate analogues.

Studying the metal dependence of the catalytic activity, we observed that xylose isomerization of PirXI can be activated by various bivalent metals, but the level of activity is dependent on the metals. The enzyme was not activated by a trivalent metal such as Al^{3+}. Previous structural studies of XI from *Arthrobacter* showed that binding of the metal at M2 and substrate binding were disturbed when the enzyme was soaked with Al^{3+} and xylose or fructose.[59,65] Such a dependence of activity on the type of metal that is bound was also observed in previous studies.[28,31,32] It seems that the class I and class II xylose isomerases have different metal preferences as they mostly show the best activity with Mg^{2+} and Mn^{2+} metal cofactors, respectively. As a class II xylose isomerase, PirXI indeed also showed the highest activity with Mn^{2+}. Here, we explore the metal dependence of the enzyme by analyzing the structural differences in PirXI reconstituted with different ligands (metals/substrate or analogues) and interpreting the effects on the enzyme activity in view of the proposed catalytic mechanism of xylose isomerases.

The isomerase mechanism includes at least three chemical steps, accompanied and enabled by proton transfer reactions: ring opening of the substrate, hydride transfer from C2 to C1 accompanied by proton transfer from O2 to O1, and ring closure (Figure 1). Structural analysis of xylose isomerase from *St. rubiginosus* showed that the reaction involves movement of one of the metals (M2, the catalytic metal) and rotation of some of the active site residues such as Asp255 and Lys289,

DOI: 10.1021/acs.biochem.7b00777
Biochemistry 2017, 56, 5991−6005

which correspond to Asp308 and Lys342, respectively, in PirXI.[26]

The His102-Asp105 pair, which is conserved throughout xylose isomerase sequences, is involved in ring opening of the substrate that is bound to M1.[26] This ring-opening step seems to be dependent on the metals that are bound to the enzyme. In the structure of PirXI with Cd^{2+} and xylose, the substrate is found in both cyclic and linear form (Figure 6A,B). This indicates a slow ring opening that led to the very low enzyme activity in the presence of Cd^{2+}. For many xylose isomerases, Cd^{2+} is reported to inhibit the enzyme reaction, probably by preventing the ring opening of the substrates as the structure with this metal shows only the cyclic form of the substrate.[26]

After linearization of the substrate M2a that is coordinated with three aspartates, a histidine, and a water molecule shifts to M2b where it now coordinates O1 and O2 of the sugar and must therefore be in the catalytically competent position.[66] The mobility of the M2 metal is supposed to aid the reaction after ring opening to facilitate isomerization in its linear form.[26,31] A structure of the catalytically most competent enzyme (Mn^{2+} and xylose bound) revealed that Mn^{2+} occupies only the M2b position of the two conformations at the M2 site (Figure 8A). This might indicate that the rapid or more complete shift of the metal from M2a to M2b contributed to the higher activity of the enzyme in the presence of Mn^{2+} compared to the other metals. The k_{cat} of PirXI−Mg^{2+} is half that of PirXI−Mn^{2+}, and in the enzyme structure with Mg^{2+}, the metal is observed at positions M2a and M2b. In the structure of PirXI−Ca^{2+}, the M2 metal is found at only the M2a position (Figure 8A). The large size of Ca^{2+} could hamper its movement, which may be one of the causes of the low rate of reaction of PirXI with this metal.

Variations in transition state stabilization of the actual hydride transfer steps among the different metals bound in the M2b site may also contribute to the observed differences in activity. Movement of the metal at position M2 does not necessarily mean that the metal can activate the enzyme. Although Ni^{2+} was found at both M2 positions, the enzyme showed no detectable activity (Figure S3B). The presence of Ni^{2+} at two distinctive M2 positions was also observed in the structure of *St. rubiginosus* XI, which is also inactive with the metal.[26] After the ring opening of the substrate, Ni^{2+} may be incapable of inducing the polarization of the catalytic water necessary to proceed with isomerization. This inhibiting effect of Ni^{2+} has been explained by the preference for square planar coordination and its high electron affinity.[26]

PirXI is also active with Fe^{2+} as the metal cofactor, and the specific activity was ∼70% of that of PirXI−Mg^{2+}. PirXI−Fe^{2+} shows two iron ions in the active site (Figure S3A). Although the reaction of PirXI in the presence this metal was performed under O_2-limited conditions, we cannot exclude the possibility of Fe^{2+} partially being oxidized to Fe^{3+}, which would influence the activity. Strong inhibition of a class II XI by iron has been described[67] and PirXI is one of a few xylose isomerases reported so far that shows activity on xylose with the Fe^{2+} cofactor.[68,69]

Binding of substrate is also dependent on the type of metal cofactor bound to PirXI. As the ionic radius of Ca^{2+} is larger (1.14 Å) than those of other metals, the carbonyl and the 2-hydroxyl of the bound xylose are shifted away from the M2 site, placing the substrate in a position that is not favorable for catalysis (Figure 8A). This could explain the extremely high K_M for xylose in the presence of Ca^{2+}, whereas it is relatively low with Mg^{2+} or Mn^{2+}. PirXI−Co^{2+} shows the highest affinity for xylose, which led it to have the highest catalytic efficiency. However, this may be hardly relevant *in vivo* as cobalt is a less abundant metal and metal content analysis showed that almost no cobalt was bound to the purified native PirXI.

While the metal cofactors influence substrate binding, the type of substrate/inhibitor seems to influence the binding of the second metal. In the crystal structure of PirXI−Mg^{2+} with either xylitol or glycerol, only position M1 is occupied by a metal. This indicates that the binding of the metal at position M2, in the case of Mg^{2+}, requires a proper binding of the substrate as observed in the PirXI−Mg^{2+}−xylose structure. The absence of metal binding at position M2 in the presence of an inhibitor such as xylitol and sorbitol has also been observed in structures of other XIs.[55,61,62]

As shown in the structure of PirXI with sorbitol, binding of a C6 sugar is different between PirXI and class I enzymes (Figure 7). Because of a bulky tryptophan at position 140, which is substituted with a Met in the class I enzymes, binding of the C6 sugar is sterically hindered in PirXI. In the structure of a class I XI from *Arthrobacter* strain B3728, it was shown that O6 of the D-sorbitol was pointing toward the methionine residue.[70] Indeed, the activity assays of PirXI show that the enzyme is barely active with glucose (very low k_{cat} and high K_M), whereas the class I enzymes have higher activity with glucose.[32] In a previous study of another class II XI from *C. thermosulfurogenes*, replacing the tryptophan with the smaller phenylalanine improved both K_M and k_{cat} of the enzyme for glucose, proving that the steric hindrance of the tryptophan was responsible for the poor activity of the enzyme toward C6 sugars. Nevertheless, this property of PirXI makes it more favorable as a specialized catalyst for lignocellulosic bioethanol production as the enzyme will be devoted to only converting xylose to xylulose.

As we have revealed the impact of various metals on the kinetic properties of PirXI, it is important to understand the *in vivo* metal binding of the enzyme and how it influences its activity. In this study, we have measured the metal content of PirXI isolated from *E. coli*. The enzyme was found to bind a mixture of several metals, and the contents were different depending on the cultures from which the enzyme was purified. This indicates that the metal contents of the overexpressed enzyme can be influenced by the intracellular metal composition as well as the enzyme−metal affinity. Therefore, measurements of xylose isomerase activities with cell-free extracts or with enzyme samples of which the metal content is not strictly controlled by reconstitution of chelator-treated apoenzyme may give results that have little significance because of variations in metal content, some of which may be introduced during sample preparation. Thus, the medium composition, expression level, and growth phase of cultures may influence metal availability and apparent XI activity.[67,69] Previously, Hlima and colleagues found that the recombinant xylose isomerase from *Streptomyces* sp. SK expressed in *E. coli* has activity lower than that of the native enzyme, which was explained by the lack of posttranslational modification.[71] However, overexpression of the recombinant enzyme could have led to the different metal contents and, hence, the different activities. In a recent study, we have shown that intracellular metal contents play a critical role for the *in vivo* activity of PirXI expressed in *S. cerevisiae* as it influences metal loading of the enzyme and, thereby, the *in vivo* catalytic activity and the rate of xylose metabolism.[33]

DOI: 10.1021/acs.biochem.7b00777
Biochemistry 2017, 56, 5991−6005

Although the total metal contents of the purified enzyme were close to the theoretical value (two metal ions per monomer of PirXI), it seems that the enzyme loses some of the metals during sample preparation for crystallization. The crystal structure of native PirXI showed that only M1 was occupied, which indicates stronger metal binding at M1 than at M2. Interestingly, His272, one of the M2 metal-coordinating residues, was shown to be doubly protonated half of the time, and this could cause weak binding of the metal,[26,58] although this could be dependent on the type of metal. The refinement of the structure with different metals at M1 showed that the occupancy of metals decreases in the following order: $Ca^{2+} > Mg^{2+} > Fe^{2+}$. Because the metal content analysis showed that the enzyme bound mainly Mg^{2+} and lower levels of Ca^{2+} and Fe^{2+}, we speculate that more Mg^{2+} was bound at M2 than at M1 in native PirXI. Different affinities of various metal ions for the M1 and M2 binding sites were also observed in previous studies, and the metal preferences differ between the isomerases. For instance, XI from *Arthrobacter* B3728 showed a high affinity for Mn^{2+}, Co^{2+}, Cd^{2+}, and Pb^{2+} at M2 and Mg^{2+} and Al^{3+} at M1, while XI from *St. rubiginosus* prefers Mg^{2+} at position M1 and other various metal ions at position M2.[26,61,70]

In the study presented here, we measured the activation constants (K_{act}) of different metals, which are probably determined by the binding site with the lower affinity. PirXI has the highest affinity for Mn^{2+}, which is also the superior metal for enzyme activity. The affinity of the enzyme for different metals does not necessarily correlate with the chemical reactivity of the metals for the isomerization reaction. Even though the K_{act} for Co^{2+} is much lower than that for Mg^{2+}, the enzyme is more active with Mg^{2+}. Interestingly, the metal binding affinity of XI from an *Arthrobacter* strain is similar to that of PirXI (Mn > Co > Mg), but this enzyme shows the highest activity in the presence of Mg^{2+}.[30] As metal binding residues in xylose isomerases are highly conserved, it is likely that the different chemical reactivity of a metal in different XIs is influenced by the overall protein environment, including second-shell residues and perhaps the residues that are farther from the active site.

The results reported here reveal clear differences between different metals with respect to the binding mode, affinity, and catalytic activity of PirXI. The various assays and crystallography experiments were performed with the apoenzyme reconstituted with different metals. Several factors, including metal-dependent PirXI activity, metal availability, and metal affinity, could affect the efficiency of the enzyme *in vivo*. It is possible that further exploration using mixtures of metals will be necessary to fully understand the *in vivo* activity of the enzyme. Previously, the activities of PirXI in the presence of metal mixtures that represented the *in vivo* metal composition of different *S. cerevisiae* strains showed that Mn^{2+} influenced the overall activity significantly, despite it being a minor component of the overall mixtures.[33] This suggests a higher affinity of the enzyme for this metal, in agreement with the current half-saturation constants (K_{act}). On the other hand, an inhibitory effect of Ca^{2+} was not pronounced at concentrations mimicking the *in vivo* levels, as the activities with the metal mixtures were as high as the activity with Mg^{2+} alone.

Besides metal content, the pH dependence of XI may be important for the *in vivo* activity. PirXI shows an optimum pH of ≥7.5 in the presence of Mg^{2+}, Mn^{2+}, and Ca^{2+}. The enzyme activity decreases rapidly at pH <6.5, and this decrease is thought to be related to the local pK_a of His272, which is involved in metal (M2) coordination, or Lys342, which in turn interacts with the metal binding residue Asp310.[26] The pH–activity profile seems also to be dependent on the metals as PirXI–Co^{2+} showed a pH profile different from that of the enzyme with other metals. The activity of PirXI–Co^{2+} is unaffected by the pH, at least in the range of 5.5–7.5. The pH profiles of xylose isomerases of different biological origin may vary. Some show the best activity in the acidic pH range,[71−74] and some are most active in the neutral pH range[3,69,75] or the basic pH range.[32,76] Comparing the sequences and structures of these XIs with different pH optima will be useful for engineering PirXI to optimize its activity for the cytosolic pH of the *S. cerevisiae*.

CONCLUSIONS

Xylose isomerase from *Piromyces* sp. E2, which catalyzes xylose isomerization in metabolically engineered *S. cerevisiae* strains for conversion of pentoses to ethanol, can accept various metals. The catalytic performance of the enzyme is dependent on the type of metal that is bound, with Mn^{2+} being the best metal, followed by Mg^{2+}. Ca^{2+} and Cd^{2+} poorly activate the reactions, and Ni^{2+} and Al^{3+} are not activating. Because there is no clear correlation between the metal-dependent activities and the affinity of the enzyme for metal ions, *in vivo* XI performance will be influenced by the availability of metal in the medium, uptake and distribution of metal in cells, and incorporation of metal into the enzyme.

Overall, the PirXI crystal structures are similar to other XI structures, the major differences being the N-terminal α-helix extension and the size of the interface area in the tetramers as compared to class I XIs. The active site of each PirXI subunit contains a substrate binding site and two metal binding sites formed by several aspartates and glutamates that are conserved throughout XIs. The results of soaking experiments confirmed that PirXI is highly promiscuous with respect to metal binding and suggest that differences in movement of the catalytic metal to a position required for hydride-shift catalysis and associated conformational changes of metal binding side chains may be related to differences in catalytic performance.

Understanding the metal-dependent catalytic properties of the enzyme through structural and biochemical studies as described in this study provides critical insights for enzyme engineering to optimize the *in vivo* enzyme activity, thereby improving the production of ethanol from xylose.

ASSOCIATED CONTENT

Supporting Information

The Supporting Information is available free of charge on the ACS Publications website at DOI: 10.1021/acs.biochem.7b00777.

Sequence alignment of xylose isomerases (Figure S1), active site structures with electron density maps (Figure S2), active site structures of Fe–XI and Ni–XLS–XI (Figure S3), and metal–ligand distances (Table S1) (PDF)

AUTHOR INFORMATION

Corresponding Author

*Groningen Biomolecular Sciences and Biotechnology Institute, University of Groningen, Nijenborgh 4, 9747 AG Groningen, The Netherlands. Telephone: 0031 50 363 4008. E-mail: d.b.janssen@rug.nl.

DOI: 10.1021/acs.biochem.7b00777
Biochemistry 2017, 56, 5991−6005

ORCID

Dick B. Janssen: 0000-0002-0834-2043

Present Address

[§]H.M.D.: c-LEcta GmbH, Perlickstr. 5, 04103 Leipzig, Germany.

Funding

This work was performed within the BE-Basic R&D Program (http://www.be-basic.org/), which is financially supported by an EOS Long-term grant from the Dutch Ministry of Economic Affairs, Agriculture and Innovation (EL&I).

Notes

The authors declare no competing financial interest.

■ ACKNOWLEDGMENTS

The authors thank Marcelo F. Masman (RUG) and Paul Klaassen (DSM) for their expert advice.

■ REFERENCES

(1) Hahn-Hägerdal, B., Karhumaa, K., Fonseca, C., Spencer-Martins, I., and Gorwa-Grauslund, M. F. (2007) Towards industrial pentose-fermenting yeast strains. *Appl. Microbiol. Biotechnol. 74*, 937−953.

(2) Sànchez Nogué, V., and Karhumaa, K. (2015) Xylose fermentation as a challenge for commercialization of lignocellulosic fuels and chemicals. *Biotechnol. Lett. 37*, 761−772.

(3) Madhavan, A., Tamalampudi, S., Ushida, K., Kanai, D., Katahira, S., Srivastava, A., Fukuda, H., Bisaria, V. S., and Kondo, A. (2009) Xylose isomerase from polycentric fungus *Orpinomyces*: gene sequencing, cloning, and expression in *Saccharomyces cerevisiae* for bioconversion of xylose to ethanol. *Appl. Microbiol. Biotechnol. 82*, 1067−78.

(4) Hector, R. E., Dien, B. S., Cotta, M. A., and Mertens, J. A. (2013) Growth and fermentation of D-xylose by *Saccharomyces cerevisiae* expressing a novel D-xylose isomerase originating from the bacterium *Prevotella ruminicola* TC2−24. *Biotechnol. Biofuels 6*, 84.

(5) Kuyper, M., Harhangi, H. R., Stave, A. K., Winkler, A. A., Jetten, M. S. M., de Laat, W. T. A. M., den Ridder, J. J. J., Op den Camp, H. J. M, van Dijken, J. P., and Pronk, J. T. (2003) High-level functional expression of a fungal xylose isomerase: the key to efficient ethanolic fermentation of xylose by *Saccharomyces cerevisiae*. *FEMS Yeast Res. 4*, 69−78.

(6) de Figueiredo Vilela, L., de Mello, V. M., Reis, V. C. B., Bon, E. P. da S., Gonçalves Torres, F. A., Neves, B. C., and Eleutherio, E. C. A. (2013) Functional expression of *Burkholderia cenocepacia* xylose isomerase in yeast increases ethanol production from a glucose-xylose blend. *Bioresour. Technol. 128*, 792−796.

(7) Matsushika, A., Inoue, H., Kodaki, T., and Sawayama, S. (2009) Ethanol production from xylose in engineered *Saccharomyces cerevisiae strains*: Current state and perspectives. *Appl. Microbiol. Biotechnol. 84*, 37−53.

(8) Walfridsson, M., Anderlund, M., Bao, X., and Hahn-Hägerdal, B. (1997) Expression of different levels of enzymes from the *Pichia stipitis*XYL1 and XYL2 genes in *Saccharomyces cerevisiae* and its effects on product formation during xylose utilisation. *Appl. Microbiol. Biotechnol. 48*, 218−224.

(9) Young, E., Lee, S., and Alper, H. (2010) Optimizing pentose utilization in yeast: the need for novel tools and approaches. *Biotechnol. Biofuels 3*, 24.

(10) Karhumaa, K., Garcia Sanchez, R., Hahn-Hägerdal, B., and Gorwa-Grauslund, M.-F. (2007) Comparison of the xylose reductase-xylitol dehydrogenase and the xylose isomerase pathways for xylose fermentation by recombinant *Saccharomyces cerevisiae*. *Microb. Cell Fact. 6*, 5.

(11) Bhosale, S. H., Rao, M. B., and Deshpande, V. V. (1996) Molecular and industrial aspects of glucose isomerase. *Microbiol. Rev. 60*, 280−300.

(12) Amore, R., Wilhelm, M., and Hollenberg, C. P. (1989) The fermentation of xylose - an analysis of the expression of *Bacillus* and *Actinoplanes* xylose isomerase genes in yeast. *Appl. Microbiol. Biotechnol. 30*, 351−357.

(13) Moes, C., Pretorius, I., and van Zyl, W. H. (1996) Cloning and expression of the *Clostridium thermosulfurogenes* D-xylose isomerase gene (xyLA) in *Saccharomyces cerevisiae*. *Biotechnol. Lett. 18*, 269−274.

(14) Sarthy, A. V., Mcconaughy, B. L., Lobo, Z., Sundstorm, J. A., Furlong, C. E., and Hall, B. D. (2000) Expression of the *Escherichia coli* xylose isomerase gene in *Saccharomyces cerevisiae*. *Appl. Environ. Microbiol. 53*, 1996−2000.

(15) Gárdonyi, M., and Hahn-Hägerdal, B. (2003) The *Streptomyces rubiginosus* xylose isomerase is misfolded when expressed in *Saccharomyces cerevisiae*. *Enzyme Microb. Technol. 32*, 252−259.

(16) Walfridsson, M., Bao, X., Anderlund, M., Lilius, G., Bülow, L., and Hahn-Hägerdal, B. (1996) Ethanolic fermentation of xylose with *Saccharomyces cerevisiae* harboring the *Thermus thermophilus* xylA gene, which expresses an active xylose (glucose) isomerase. *Appl. Environ. Microbiol. 62*, 4648−4651.

(17) Harhangi, H., Akhmanova, A. S., Emmens, R., van der Drift, C., de Laat, W. T. A. M., van Dijken, J. P., Jetten, M. S. M., Pronk, J. T., and Op den Camp, H. J. M. (2003) Xylose metabolism in the anaerobic fungus *Piromyces* sp. strain E2 follows the bacterial pathway. *Arch. Microbiol. 180*, 134−141.

(18) van Maris, A. J. A., Winkler, A. A., Kuyper, M., de Laat, W. T. A. M., van Dijken, J. P., and Pronk, J. T. (2007) Development of efficient xylose fermentation in *Saccharomyces cerevisiae*: xylose isomerase as a key component. *Adv. Biochem. Eng./Biotechnol. 108*, 179−204.

(19) Brat, D., Boles, E., and Wiedemann, B. (2009) Functional expression of a bacterial xylose isomerase in *Saccharomyces cerevisiae*. *Appl. Environ. Microbiol. 75*, 2304−11.

(20) Zhou, H., Cheng, J.-s., Wang, B. L., Fink, G. R., and Stephanopoulos, G. (2012) Xylose isomerase overexpression along with engineering of the pentose phosphate pathway and evolutionary engineering enable rapid xylose utilization and ethanol production by *Saccharomyces cerevisiae*. *Metab. Eng. 14*, 611−622.

(21) Kuyper, M., Hartog, M. M. P., Toirkens, M. J., Almering, M. J. H., Winkler, A. A., van Dijken, J. P., and Pronk, J. T. (2005) Metabolic engineering of a xylose-isomerase-expressing *Saccharomyces cerevisiae* strain for rapid anaerobic xylose fermentation. *FEMS Yeast Res. 5*, 399−409.

(22) Wisselink, H. W., Toirkens, M. J., del Rosario Franco Berriel, M., Winkler, A. A., van Dijken, J. P., Pronk, J. T., and Van Maris, A. J. A. (2007) Engineering of *Saccharomyces cerevisiae* for efficient anaerobic alcoholic fermentation of L-arabinose. *Appl. Environ. Microbiol. 73*, 4881−4891.

(23) Kuyper, M., Toirkens, M. J., Diderich, J. A., Winkler, A. A., van Dijken, J. P., and Pronk, J. T. (2005) Evolutionary engineering of mixed-sugar utilization by a xylose-fermenting *Saccharomyces cerevisiae* strain. *FEMS Yeast Res. 5*, 925−34.

(24) Lee, S. M., Jellison, T., and Alper, H. S. (2012) Directed evolution of xylose isomerase for improved xylose catabolism and fermentation in the yeast *Saccharomyces cerevisiae*. *Appl. Environ. Microbiol. 78*, 5708−16.

(25) Fuxreiter, M., Farkas, Ö., and Náray-Szabó, G. (1995) Molecular modelling of xylose isomerase catalysis: The role of electrostatics and charge transfer to metals. *Protein Eng., Des. Sel. 8*, 925−933.

(26) Kovalevsky, A. Y., Hanson, L., Fisher, S. Z., Mustyakimov, M., Mason, S. A., Trevor Forsyth, V., Blakeley, M. P., Keen, D. A., Wagner, T., Carrell, H. L., Katz, A. K., Glusker, J. P., and Langan, P. (2010) Metal ion roles and the movement of hydrogen during reaction catalyzed by D-xylose isomerase: A joint x-ray and neutron diffraction study. *Structure 18*, 688−699.

(27) Fuxreiter, M., Böcskei, Z., Szeibert, A., Szabó, E., Dallmann, G., Náray-Szabó, G., and Asbóth, B. (1997) Role of electrostatics at the catalytic metal binding site in xylose isomerase action: Ca^{2+}-inhibition and metal competence in the double mutant D254E/D256E. *Proteins: Struct., Funct., Genet. 28*, 183−193.

DOI: 10.1021/acs.biochem.7b00777
Biochemistry 2017, 56, 5991−6005

(28) van Bastelaere, P. B. M., Vangrysperre, W., and Kersters-Hilderson, H. (1991) Kinetic studies of Mg^{2+}-, Co^{2+}- and Mn^{2+}-activated D-xylose isomerases. *Biochem. J. 278*, 285−292.
(29) Callens, M., Tomme, P., Kersters-Hilderson, H., Cornelis, R., Vangrysperre, W., and De Bruyne, C. K. (1988) Metal ion binding to D-xylose isomerase from *Streptomyces violaceoruber*. *Biochem. J. 250*, 285−290.
(30) Rangarajan, M., and Hartley, B. S. (1992) Mechanism of D-fructose isomerization by *Arthrobacter* D-xylose isomerase. *Biochem. J. 283*, 223−233.
(31) van Tilbeurgh, H., Jenkins, J., Chiadmi, M., Janin, J., Wodak, S. J., Mrabet, N. T., and Lambeir, A. M. (1992) Protein engineering of xylose (glucose) isomerase from *Actinoplanes missouriensis*. 3. Changing metal specificity and the pH profile by site- directed mutagenesis. *Biochemistry 31*, 5467−5471.
(32) Smith, C., Rangarajan, M., and Hartley, B. (1991) D-Xylose (D-glucose) isomerase from *Arthrobacter* strain NRRL B3728. Purification and properties. *Biochem. J. 277*, 255−261.
(33) Verhoeven, M. D., Lee, M., Kamoen, L., van den Broek, M., Janssen, D. B., Daran, J.-M. G., van Maris, A. J. A., and Pronk, J. T. (2017) Mutations in PMR1 stimulate xylose isomerase activity and anaerobic growth on xylose of engineered *Saccharomyces cerevisiae* by influencing manganese homeostasis. *Sci. Rep. 7*, 46155.
(34) Han, B., Bong, S. M., Cho, J., Kim, M., Kim, S. J., and Lee, B. I. (2015) Crystal structure of a Class 2 D-xylose isomerase from the human intestinal tract microbe *Bacteroides thetaiotaomicron*. *Bio Design 289*, 41−47.
(35) Yamanaka, K. (1974) Enzymatic assay of D-xylose isomerase with D-sorbitol dehydrogenase. *Agric. Biol. Chem. 38*, 2035−2037.
(36) Matthews, B. W. (1968) Solvent content of protein crystals. *J. Mol. Biol. 33*, 491−497.
(37) Berejnov, V., Husseini, N. S., Alsaied, O. A., and Thorne, R. E. (2006) Effects of cryoprotectant concentration and cooling rate on vitrification of aqueous solutions. *J. Appl. Crystallogr. 39*, 244−251.
(38) Battye, T. G. G., Kontogiannis, L., Johnson, O., Powell, H. R., and Leslie, A. G. W. (2011) iMOSFLM: A new graphical interface for diffraction-image processing with MOSFLM. *Acta Crystallogr., Sect. D: Biol. Crystallogr. 67*, 271−281.
(39) Evans, P. R., and Murshudov, G. N. (2013) How good are my data and what is the resolution? *Acta Crystallogr., Sect. D: Biol. Crystallogr. 69*, 1204−1214.
(40) McCoy, A. J., Grosse-Kunstleve, R. W., Adams, P. D., Winn, M. D., Storoni, L. C., and Read, R. J. (2007) Phaser crystallographic software. *J. Appl. Crystallogr. 40*, 658−674.
(41) Langer, G. G., Cohen, S. X., Lamzin, V. S., and Perrakis, A. (2008) Automated macromolecular model building for X-ray crystallography using ARP/wARP version 7. *Nat. Protoc. 3*, 1171−1179.
(42) Emsley, P., Lohkamp, B., Scott, W. G., and Cowtan, K. (2010) Features and development of Coot. *Acta Crystallogr., Sect. D: Biol. Crystallogr. 66*, 486−501.
(43) Murshudov, G. N., Skubák, P., Lebedev, A. A., Pannu, N. S., Steiner, R. A., Nicholls, R. A., Winn, M. D., Long, F., and Vagin, A. A. (2011) REFMAC5 for the refinement of macromolecular crystal structures. *Acta Crystallogr., Sect. D: Biol. Crystallogr. 67*, 355−367.
(44) Adams, P. D., Afonine, P. V., Bunkóczi, G., Chen, V. B., Davis, I. W., Echols, N., Headd, J. J., Hung, L. W., Kapral, G. J., Grosse-Kunstleve, R. W., McCoy, A. J., Moriarty, N. W., Oeffner, R., Read, R. J., Richardson, D. C., Richardson, J. S., Terwilliger, T. C., and Zwart, P. H. (2010) PHENIX: A comprehensive Python-based system for macromolecular structure solution. *Acta Crystallogr., Sect. D: Biol. Crystallogr. 66*, 213−221.
(45) Chen, V. B., Arendall, W. B., Headd, J. J., Keedy, D. A., Immormino, R. M., Kapral, G. J., Murray, L. W., Richardson, J. S., and Richardson, D. C. (2010) MolProbity: All-atom structure validation for macromolecular crystallography. *Acta Crystallogr., Sect. D: Biol. Crystallogr. 66*, 12−21.
(46) Krissinel, E., and Henrick, K. (2004) Secondary-structure matching (SSM), a new tool for fast protein structure alignment in three dimensions. *Acta Crystallogr., Sect. D: Biol. Crystallogr. 60*, 2256−2268.
(47) Robert, X., and Gouet, P. (2014) Deciphering key features in protein structures with the new ENDscript server. *Nucleic Acids Res. 42*, W320−W324.
(48) Sugahara, M., Mizohata, E., Nango, E., Suzuki, M., Tanaka, T., Masuda, T., Tanaka, R., Shimamura, T., Tanaka, Y., Suno, C., Ihara, K., Pan, D., Kakinouchi, K., Sugiyama, S., Murata, M., Inoue, T., Tono, K., Song, C., Park, J., Kameshima, T., Hatsui, T., Joti, Y., Yabashi, M., and Iwata, S. (2014) Grease matrix as a versatile carrier of proteins for serial crystallography. *Nat. Methods 12*, 61−63.
(49) Pei, J., Kim, B.-H., and Grishin, N. V. (2008) PROMALS3D: a tool for multiple protein sequence and structure alignments. *Nucleic Acids Res. 36*, 2295−300.
(50) Gouet, P., Courcelle, E., Stuart, D., and Metoz, F. (1999) ESPript: analysis of multiple sequence alignments in PostScript. *Bioinformatics 15*, 305−308.
(51) Allen, K. N., Lavie, A., Glasfeld, A., Tanada, T. N., Gerrity, D. P., Carlson, S. C., Farber, G. K., Petsko, G. A., and Ringe, D. (1994) Role of the divalent metal ion in sugar binding, ring opening, and isomerization by D-xylose isomerase: replacement of a catalytic metal by an amino acid. *Biochemistry 33*, 1488−94.
(52) Valli, M., Sauer, M., Branduardi, P., Borth, N., Porro, D., and Mattanovich, D. (2005) Intracellular pH distribution in *Saccharomyces cerevisiae* cell populations, analyzed by flow cytometry. *Appl. Environ. Microbiol. 71*, 1515−1521.
(53) Palmqvist, E., and Hahn-Hägerdal, B. (2000) Fermentation of lignocellulosic hydrolysates. II: inhibitors and mechanisms of inhibition. *Bioresour. Technol. 74*, 25−33.
(54) Harding, M. M. (2001) Geometry of metal−ligand interactions in proteins. *Acta Crystallogr., Sect. D: Biol. Crystallogr. 57*, 401−411.
(55) Whitlow, M., Howard, A. J., Finzel, B. C., Poulos, T. L., Winborne, E., and Gilliland, G. L. (1991) A metal-mediated hydride shift mechanism for xylose isomerase based on the 1.6 Å *Streptomycs rubiginosus* structure with xylitol and D-xylose. *Proteins: Struct., Funct., Genet. 9*, 153−173.
(56) Rozeboom, H. J., Yu, S., Madrid, S., Kalk, K. H., Zhang, R., and Dijkstra, B. W. (2013) Crystal structure of α-1,4-glucan lyase, a unique glycoside hydrolase family member with a novel catalytic mechanism. *J. Biol. Chem. 288*, 26764−74.
(57) Kovalevsky, A. Y., Katz, A. K., Carrell, H. L., Hanson, L., Mustyakimov, M., Fisher, S. Z., Coates, L., Schoenborn, B. P., Bunick, G. J., Glusker, J. P., and Langan, P. (2008) Hydrogen location in stages of an enzyme-catalyzed reaction: Time-of-flight neutron structure of D-xylose isomerase with bound D-xylulose. *Biochemistry 47*, 7595−7597.
(58) Katz, A. K., Li, X., Carrell, H. L., Hanson, B. L., Langan, P., Coates, L., Schoenborn, B. P., Glusker, J. P., and Bunick, G. J. (2006) Locating active-site hydrogen atoms in D-xylose isomerase: time-of-flight neutron diffraction. *Proc. Natl. Acad. Sci. U. S. A. 103*, 8342−7.
(59) Collyer, C. A., Henrick, K., and Blow, D. M. (1990) Mechanism for aldose-ketose interconversion by D-xylose isomerase involving ring opening followed by a 1,2-hydride shift. *J. Mol. Biol. 212*, 211−235.
(60) Garcia-Viloca, M., Alhambra, C., Truhlar, D. G., and Gao, J. (2003) Hydride transfer catalyzed by xylose isomerase: Mechanism and quantum effects. *J. Comput. Chem. 24*, 177−190.
(61) Collyer, C. A., and Blow, D. M. (1990) Observations of reaction intermediates and the mechanism of aldose-ketose interconversion by D-xylose isomerase. *Proc. Natl. Acad. Sci. U. S. A. 87*, 1362−6.
(62) Jenkins, J., Janin, J., Rey, F., Chiadmi, M., van Tilbeurgh, H., Lasters, I., de Maeyer, M., Ven Belle, D., Wodak, S. J., Lauwereys, M., Stanssens, P., Mrabet, N. T., Snauwaert, J., Matthyssens, G., and Lambeir, A. (1992) Protein engineering of xylose (glucose) isomerase from *Actinoplanes missouriensis*. 1. Crystallography and site-directed mutagenesis of metal binding sites. *Biochemistry 31*, 5449−5458.
(63) Kovalevsky, A., Hanson, B. L., Mason, S. A., Forsyth, V. T., Fisher, Z., Mustyakimov, M., Blakeley, M. P., Keen, D. A., and Langan, P. (2012) Inhibition of D-xylose isomerase by polyols: atomic details

DOI: 10.1021/acs.biochem.7b00777
Biochemistry 2017, 56, 5991−6005

by joint X-ray/neutron crystallography. *Acta Crystallogr., Sect. D: Biol. Crystallogr. 68*, 1201−6.
(64) Carrell, H. L., Hoier, H., and Glusker, J. P. (1994) Modes of binding substrates and their analogues to the enzyme D-xylose isomerase. *Acta Crystallogr., Sect. D: Biol. Crystallogr. 50*, 113−123.
(65) Gérczei, T., Böcskei, Z., Szabó, E., Asbóth, B., and Náray-Szabó, G. (1999) Structure determination and refinement of the Al^{3+} complex of the D254,256E mutant of *Arthrobacter* D -xylose isomerase at 2.40 Å resolution. Further evidence for inhibitor-induced metal ion movement. *Int. J. Biol. Macromol. 25*, 329−336.
(66) Fenn, T. D., Ringe, D., and Petsko, G. A. (2004) Xylose isomerase in substrate and inhibitor michaelis states: atomic resolution studies of a metal-mediated hydride shift. *Biochemistry 43*, 6464−74.
(67) Karaoglu, H., Yanmis, D., Sal, F. A., Celik, A., Canakci, S., and Belduz, A. O. (2013) Biochemical characterization of a novel glucose isomerase from *Anoxybacillus gonensis* G2T that displays a high level of activity and thermal stability. *J. Mol. Catal. B: Enzym. 97*, 215−224.
(68) Callens, M., Kersters-Hilderson, H., Van Opstal, O., and De Bruyne, C. K. (1986) Catalytic properties of D-xylose isomerase from *Streptomyces violaceoruber*. *Enzyme Microb. Technol. 8*, 696−700.
(69) Lee, C. Y., and Zeikus, J. G. (1991) Purification and characterization of thermostable glucose isomerase from *Clostridium thermosulfurogenes* and *Thermoanaerobacter* strain B6A. *Biochem. J. 273*, 565−571.
(70) Henrick, K., Collyer, C. A., and Blow, D. M. (1989) Structures of D-xylose isomerase from *Arthrobacter* strain B3728 containing the inhibitors xylitol and D-sorbitol at 2.5 Å and 2.3 Å resolution, respectively. *J. Mol. Biol. 208*, 129−157.
(71) Ben Hlima, H., Ayadi, D., Aghajari, N., and Bejar, S. (2013) Differential properties of native and tagged or untagged recombinant glucose isomerases of *Streptomyces* sp. SK and possible implication of the glycosylation. *J. Mol. Catal. B: Enzym. 94*, 82−87.
(72) Staudigl, P., Haltrich, D., and Peterbauer, C. K. (2014) L-arabinose isomerase and D-xylose isomerase from *Lactobacillus reuteri*: Characterization, coexpression in the food grade host *Lactobacillus plantarum*, and application in the conversion of D-galactose and D-glucose. *J. Agric. Food Chem. 62*, 1617−1624.
(73) Srih-Belghith, K., and Bejar, S. (1998) A thermostable glucose isomerase having a relatively low optimum pH: Study of activity and molecular cloning of the corresponding gene. *Biotechnol. Lett. 20*, 553−556.
(74) Liu, S. Y., Wiegel, J., and Gherardini, F. C. (1996) Purification and cloning of a thermostable xylose (glucose) isomerase with an acidic pH optimum from *Thermoanaerobacterium* strain JW/SL-YS 489. *J. Bacteriol. 178*, 5938−5945.
(75) van Bastelaere, P. B. M., Kersters-Hilderson, H. L. M., and Lambeir, A. M. (1995) Wild-type and mutant D-xylose isomerase from *Actinoplanes missouriensis*: metal-ion dissociation constants, kinetic parameters of deuterated and non-deuterated substrates and solvent-isotope effects. *Biochem. J. 307*, 135−142.
(76) Cha, J., and Batt, C. (1998) Lowering the pH optimum of D-xylose isomerase: the effect of mutations of the negatively charged residues. *Mol. Cells 8*, 374−382.

DOI: 10.1021/acs.biochem.7b00777
Biochemistry 2017, 56, 5991−6005